Original Article

Imaging anatomy of the vidian canal and its clinical significance

Wanyang Gong[1], Wei Cao[2], Wei Zhang[1,3,4,5], Rong Xiang[1,3,4,5], Yu Xu[1,3,4,5]

[1]Department of Otolaryngology-Head and Neck Surgery, Renmin Hospital of Wuhan University, Wuhan, China; [2]Department of Otolaryngology, Huangshi Central Hospital, Huangshi, China; [3]Research Institute of Otolaryngology-Head and Neck Surgery, Renmin Hospital of Wuhan University, Wuhan, China; [4]Department of Rhinology and Allergy, Renmin Hospital of Wuhan University, Wuhan, China; [5]Hubei Province Key Laboratory of Allergy and Immunology, Wuhan, China

Contributions: (I) Conception and design: W Gong; (II) Administrative support: Y Xu; (III) Provision of study materials or patients: W Cao, W Zhang, R Xiang, Y Xu; (IV) Collection and assembly of data: W Gong, W Cao; (V) Data analysis and interpretation: W Gong; (VI) Manuscript writing: All authors; (VII) Final approval of manuscript: All authors.

Correspondence to: Yu Xu, PhD. Department of Otolaryngology-Head and Neck Surgery, Renmin Hospital of Wuhan University, 238 Jiefang Road, Wuhan 430060, China; Research Institute of Otolaryngology-Head and Neck Surgery, Renmin Hospital of Wuhan University, Wuhan, China; Department of Rhinology and Allergy, Renmin Hospital of Wuhan University, Wuhan, China; Hubei Province Key Laboratory of Allergy and Immunology, Wuhan, China. Email: xuy@whu.edu.cn.

Background: Vidian neurectomy (VN) is an effective surgical treatment for severe allergic rhinitis (AR). However, little research has been conducted on the imaging anatomy of the vidian canal (VC). This study aimed to analyze the computed tomography (CT) imaging of the VC and its surrounding structures and investigate the morphometric characteristics and clinical significance of VN.

Methods: We analyzed 118 paranasal sinus CT scans (55 male and 63 female patients), with axial, coronal, and sagittal slices being used in the study.

Results: Among the 118 patients in this study, the average length of the VC in male and female patients was 14.00±3.35 and 12.51±3.42 mm, respectively; the transverse diameter of the posterior segment of the VC in females was larger than that in males; and the length of the VC and the distance between VC and foramen rotundum (FR) in males were longer than those in females. The angle between the VC and the sagittal plane and the angle between the sphenopalatine foramen (SPF) and the VC in females were larger than those in males, and the distance between the attachment to the end of the middle turbinate (MT) and the VC was greater. Type 2 VC occupied a dominant position. The VC was mostly at the same line as the medial wall of the maxillary sinus (MS) and was located on the medial side of the medial pterygoid plate (MPTG). The highest point of the VC was mostly superior to that of the palatovaginal canal (PVC). Most of the VC was inferior to the internal carotid artery (ICA), and no cases were observed in which the VC was above the ICA. Some of the measurements of the VC and its surrounding structures were correlated.

Conclusions: The position and morphometric information of the VC could be reflected in a CT scan, which may contribute to the evaluation of VN preoperatively and postoperatively.

Keywords: Allergic rhinitis (AR); vidian neurectomy (VN); computed tomography image (CT image); anatomical variation

Submitted Jul 20, 2023. Accepted for publication Oct 12, 2023. Published online Oct 25, 2023.
doi: 10.21037/qims-23-1033
View this article at: https://dx.doi.org/10.21037/qims-23-1033

Introduction

The prevalence of allergic rhinitis (AR) has been increasing in recent years (1-3). As reported in a clinical and pathophysiological overview, more than 400 million people in the world experience AR, arousing concern in several fields (1-4). AR seriously affects an individuals' quality of life, severely impact a patient's work, study, social interactions, etc. (5). According to the literature, in addition to the direct medical expenses, the indirect economic loss caused by AR has even exceeded that of asthma in recent years, and thus AR poses a considerable social challenge (5,6). Vidian neurectomy (VN) to improve nasal hypersecretion is the main surgical treatment for moderate to severe AR (7,8). This operation can also contribute to the treatment of intractable vasomotor rhinitis (VMR) (9) and has a significant clinical effect in alleviating the symptoms of patients with refractory rhinitis, improving their quality of life, and reducing the use of drugs (10-12).

VN was first proposed by Golding-Wood for the treatment of VMR (11,13). However, it could not be widely promoted owing to its associated surgical trauma, difficult exposure to the surgical field, and multiple complications. Recently, with the development of technology and the exploration of the fine anatomy around the vidian canal (VC), the incidence of complications has been reduced. VN has been reapplied clinically and become one of the most widely used surgical treatments for AR and VMR (7,9,12). Precisely locating the anterior opening of the VC plays a key role in approaching the vidian nerve through the middle nasal meatus in VN, as this can reduce surgical injury, avoid complications, and shorten the operation time. Therefore, it is crucial to locate the anterior opening of VC through the surrounding structures, such as the sphenopalatine foramen (SPF), the palatovaginal canal (PVC), the end of the middle turbinate (MT), and the medial pterygoid plate (MPTG) (*Figure 1*). As the most common preoperative examination method in clinical practice, computed tomography (CT) is critical to VN. However, there are few reports on the imaging anatomy of the VC and its surrounding structures based on the surgical operation in clinical practice.

In this study, we examined whether the use of CT could contribute the risk assessment, intraoperative navigation, and protection of important adjacent structures during VN. Additionally, we characterized the imaging anatomy of the VC and its relative position to the surrounding structures to explore the value of scan in the preoperative localization and risk assessment of VN. This study firstly reported on the relative position between the maxillary sinus (MS) and the VC and the first to jointly consider the surgical significance of the structures surrounding VC. We hope our findings can serve as a reference for preoperative assessment in subsequent clinical practice. We present this article in accordance with the STROBE reporting checklist (available at https://qims.amegroups.com/article/view/10.21037/qims-23-1033/rc).

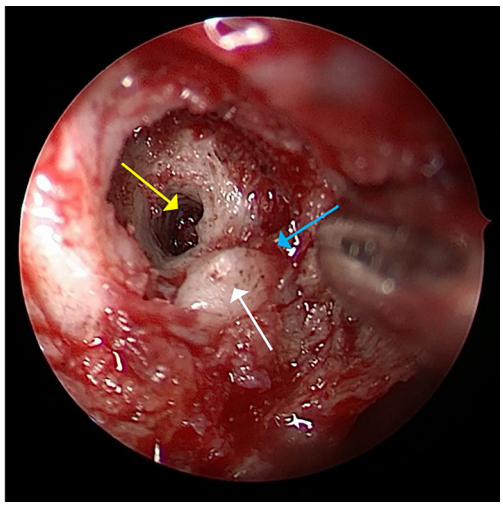

Figure 1 Endoscopic findings in VN. Yellow arrow: the anterior opening of the VC; white arrow: MPTG; blue arrow: PVC. VN, vidian neurectomy; VC, vidian canal; MPTG, medial pterygoid plate; PVC, palatovaginal canal.

Methods

Clinical data

A retrospective analysis was conducted on paranasal sinus CT scans from 118 patients (55 males and 63 females) between January 2018 and January 2019 in Renmin Hospital of Wuhan University. These patients underwent sinus CT scans for different conditions, such as headache, nasal symptoms, maxillofacial discomfort, eye discomfort, and preoperative evaluation of endoscopic dacryocystorhinostomy. The exclusion criteria were as follows: (I) a history of facial trauma, fracture, or deformity; (II) a history of previous surgery on the sinus or skull base; (III) a history of paranasal sinus tumors or other conditions affecting the imaging analysis; and (IV) interrupted continuity of the VC or one that could not be identified clearly. The study was conducted in accordance with the Declaration of Helsinki (as revised in 2013) and was approved by the Ethics Committee of Renmin Hospital

of Wuhan University (No. WDRY2022-K237). The requirement for informed consent for this study was waived due to its retrospective nature.

CT scanning, reconstruction, and observation

CT scanning was performed using the Light Speed GE 64 slice spiral CT system (GE HealthCare, Chicago, IL, USA). The scanning range was from the superior margin of the frontal sinus to the inferior margin of the maxillary alveolar process, and the scanning layer thickness was 0.5 mm. CT scans were obtained under the following parameters: 0.625-mm section thickness, 0.5-mm intervals, 120–320 mA, and 120 kV. Centricity Enterprise Web 3.0 (GE HealthCare) imaging system was used for observation and measurement. The intermediate window and level settings were 2,000 and 350 Hounsfield units (HU), respectively. The images were independently measured and analyzed by two doctors, and the average value was taken from three data measurements.

Measurements and definitions of each type and relative positional relationship

The VC was located in the axial plane, and the following values were measured: the length of the VC; the diameter of the anterior, central, and posterior segment of the VC; and the angle between the VC and the sagittal plane. Considering that SPF is adjacent to the VC and is a significant anatomical landmark in VN, the transverse diameter of the SPF, the distance between the medial border of the anterior boundary of the VC to the posterior boundary of the SPF, and the angle between the axis of the SPF to the axis of the VC were measured. For the same reason, we located the PVC in the axial plane and measured the angle between the axis of the PVC and the VC (*Figure 2*), the distance from the posterior wall of the MS to the VC (*Figure 2*), and the distance from the attachment of the end of the MT to the VC. Due to the close location of the foramen rotundum (FR), we measured the shortest distance between the VC and the FR in the coronal plane in order to protect the maxillary nerve in VN (*Figure 2*).

The relative positions between the VC and other structures were as follows. The position of the VC was identified as online, medial, or lateral to the medial wall of the MS (*Figure 3*); the position of the PVC was identified as inferior, at, or superior to the VC (*Figure 4*); the MPTG was determined to be at the coronal plane; and the VC was identified to be online, medial, or lateral to the MPTG (*Figure 5*). In regard to the petrous internal carotid artery (pICA), the position of the VC was identified as inferior, at, or superior to the pICA (*Figure 6*).

According to the research of Açar *et al.* (14) and Vuksanovic-Bozaric *et al.* (15), the VC was classified into three types based on its localization: type 1, the VC was located inside the roof of the pterygopalatine fossa (PPF); type 2, the VC was partially protruding into the sphenoid sinus; and type 3, the was VC completely protruding into the sphenoid sinus, with a stalk connecting it to the PPF roof (*Figure 7*).

Based on the evaluation of sphenoid sinus in the report of Rahmati *et al.* (6), the sphenoid sinuses were categorized into four types depending on the position of the sinus relative to the sella turcica: type I, conchal (completely missing or minimal sphenoid sinus); type II, presellar (posterior wall of the sphenoid sinus in front of the anterior wall of the sella); type III, sellar (posterior wall located between the anterior and posterior wall of the sella); and type IV, postsellar (posterior wall of the sphenoid sinus located behind the posterior wall of the sella) (*Figure 8*).

According to Zhou *et al.* (16) and Cao *et al.* (17), the anatomical variation of posterior ethmoidal cells, which may be related to the VC, could be classified as ethmomaxillary sinus (EMS), retromaxillary air cell (RMC), and Haller cell (located below the orbit and above the MS) and without any infraorbital cells (*Figure 9*).

Statistical methods

SPSS 22.0 software (IBM Corp., Armonk, NY, USA) was used for statistical analysis. A two-way mixed-effects single measures intraclass correlation coefficient (ICC) analysis was conducted to assess the interobserver agreement. The normal distribution was evaluated using the Kolmogorov-Smirnov (K-S) single-sample test combined with observation via histogram and scatter plot. When the results of the K-S test were inconsistent with those of the histogram and scatter plot, the results of the latter prevailed. The independent sample *t*-test, chi-squared test, and Fisher exact test were used to analyze the differences between groups. Correlation analysis was performed using Pearson correlation or Spearman correlation analysis depending on whether or not the data were consistent with a normal distribution. Logistic regression was used to analyze the related factors of classified variables, and multiple linear regression was used to analyze the related factors of

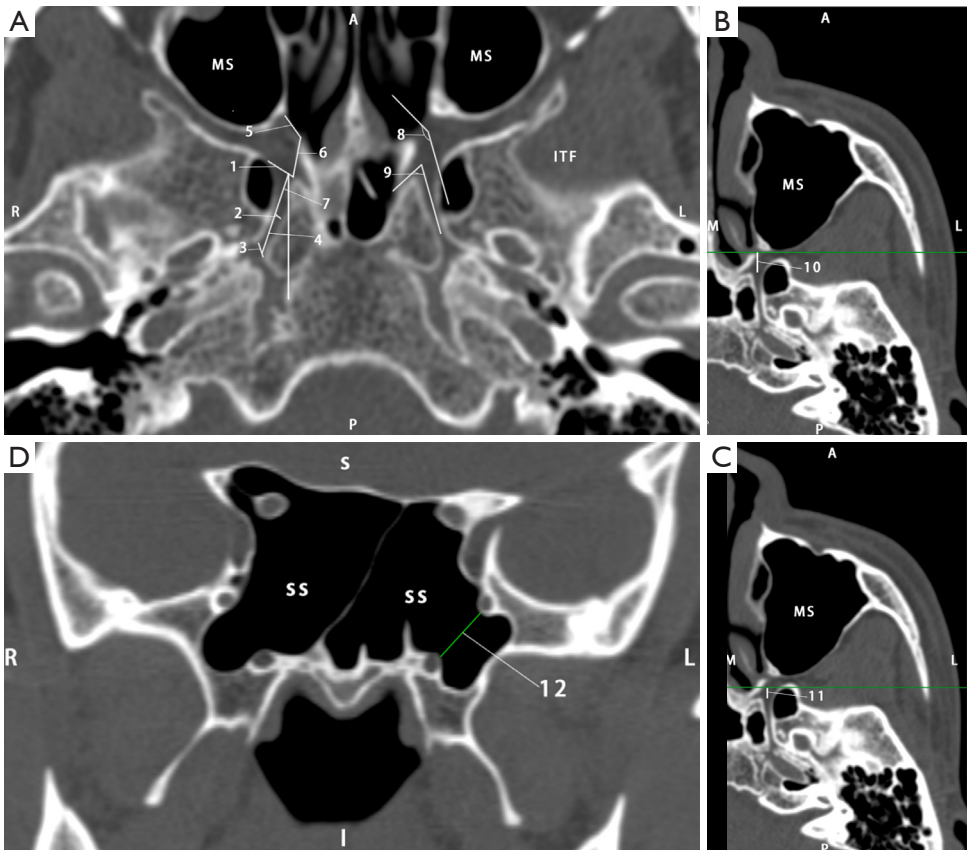

Figure 2 Definition and measurement of different values. (A) Axial slices (level of the vidian canal): the diameter of the anterior [1], central [2], and posterior [3] segment of the VC; the length of the VC [4]; the transverse diameter of the SPF [5]; the distance between the medial border of the anterior boundary of the VC to the posterior boundary of the SPF [6]; the angle between the axis of the SPF to the axis of the VC [7]; the angle between the axis of the SPF and the VC [8]; the angle between the axis of the PVC and the VC [9]. (B,C) The axial slices (level of the vidian canal) with a horizontal line drawn past the posterior wall of the MS to determine the distance from the MS to the VC [10] and a horizontal line drawn past the attachment of the end of the middle turbinate to determine the distance from the MT to the VC [11]. (D) Coronal slices (level of the vidian canal): shortest distance between the VC and the FR [12]. A, anterior; P, posterior; R, right; L, left (in A and D); MS, maxillary sinus; ITF, infratemporal fossa; L, lateral (in B and C); M, medial; S, superior; I, inferior; SS, sphenoid sinus; VC, vidian canal; SPF, sphenopalatine foramen; PVC, palatovaginal canal; MT, middle turbinate; FR, foramen rotundum.

continuous variables. Significance was defined as $P<0.05$.

Results

Table 1 displays the demographic characteristics of patients involved in this study, and the measurements of the VC and its surrounding structures, which are continuous variables, are shown in *Table 2*. *Table 3* shows the results of ICC analysis of these measures.

According to the K-S tests, the results that were consistent with a normal distribution included the angle between the VC and the sagittal plane, the distance between the anterior boundary of the VC to the SPF, the angle between the axis of the SPF and the VC, the angle between the PVC and the VC, and the shortest distance between the VC and the FR.

There were significant differences between male and female patients in the length of the VC and the diameter of the anterior, central, and posterior segment of the VC; the angle between the VC and the sagittal plane; the diameter of the SPF; the distance between the VC to the SPF; the distance between the SPF and the posterior wall of MS; and the distance between the VC and the FR ($P<0.05$) (*Table 2*).

Among the 118 patients, type 2 VC accounted for the

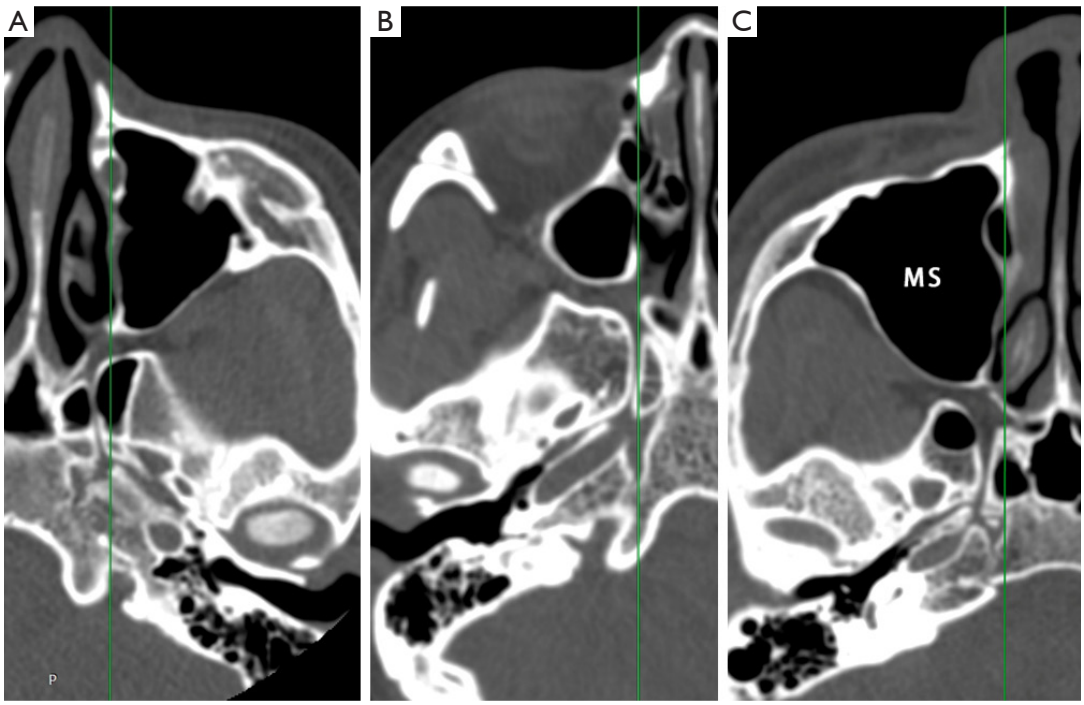

Figure 3 Axial slices with a straight line drawn along the medial wall of the MS and the position of the VC being identified as lateral (A), online (B), or medial (C) to the medial wall of the MS. P, posterior, MS, maxillary sinus; VC, vidian canal.

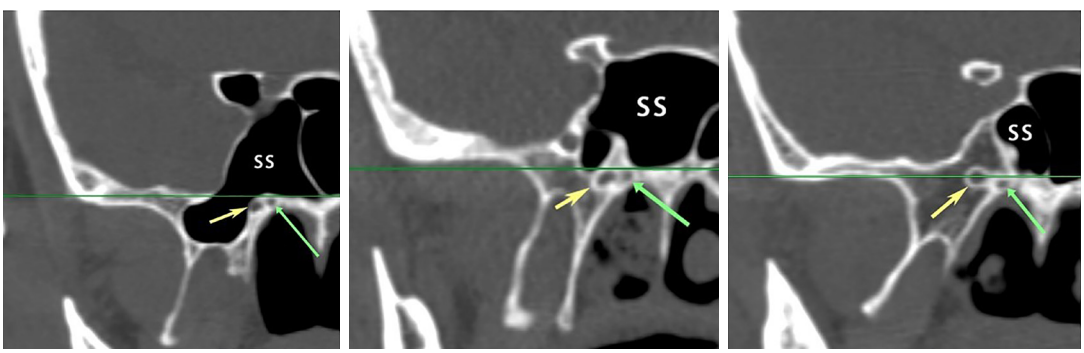

Figure 4 The coronal slices (level of the anterior boundary of the vidian canal) with a horizontal line drawn past the highest point of the PVC and the position of the VC being identified as inferior, at, or superior to the PVC. The yellow arrows indicate VC, and the green arrows indicate PVC. SS, sphenoid sinus; PVC, palatovaginal canal; VC, vidian canal.

largest proportion of cases at 60.17%, followed by type 3 at 35.17%, and type 1 at 4.66%. The difference in VC type between men and women was statistically significant (P<0.001) (*Table 4*).

Regarding the pneumatization of the sphenoid sinus, type 4 SS was predominant, accounting for 49.58% of cases, with types 2 and type 3 SS accounting for 13.98% and 36.44%, respectively; no type 1 SS was observed in this study (*Table 5*).

Our assessment of the anatomical variation of ethmoidal cells showed that RMC dominated (about 77.97%), followed by EMS (10.17%). Moreover, there were a few patients without relative anatomical variation (5.08%), and there was no significant difference between males and females (*Table 6*).

As for the position of VC relative to the medial wall

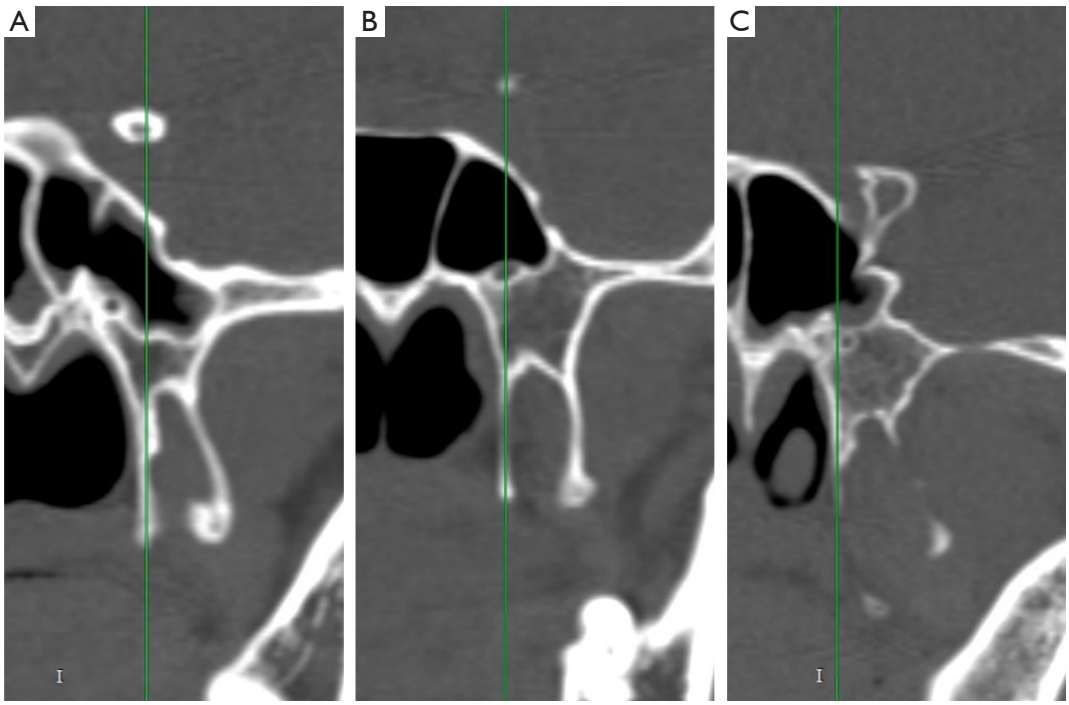

Figure 5 The coronal slices (level of the anterior boundary of the vidian canal) with a straight line drawn along the MPTG and the VC identified as medial (A), online (B), or lateral (C) to the MPTG. I, inferior; MPTG, medial pterygoid plate; VC, vidian canal.

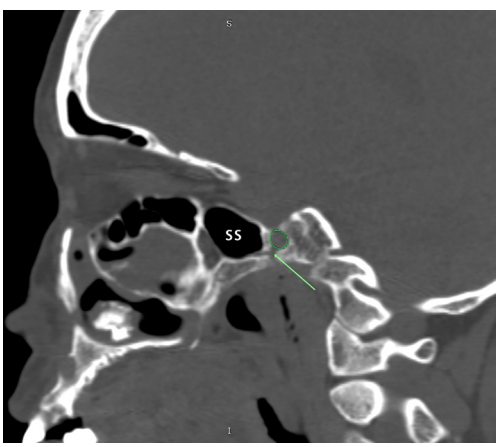

Figure 6 Coronal slices centered on the terminal aspect of the VC (green arrow) and the VC being identified as inferior, at, or superior to the pICA (green circle). S, superior; I, inferior; SS, sphenoid sinus; VC, vidian canal; pICA, petrous internal carotid artery.

of the MS, the online position for accounted for 19.92% in males and 27.97% in females, of cases, followed by the lateral position at 18.64% in males and 20.34% in females and the medial position at only 8.05% in males and 5.08% in females. The difference between males and females was not significant (*Table* 7).

The highest point of the anterior opening of the VC was superior to that of the PVC from the coronal plane in about 65.25% of cases, on the same line in 21.19%, and inferior to the PVC in 13.56%. There was no significant difference between male and female patients in this regard (*Table* 7).

No case was observed with the terminal aspect of the VC above the pICA. Most of the VCs (63.56%) were inferior to the pICA, with the others cases (36.44%) being online. The difference between male and female patients was significant ($P<0.05$) (*Table* 7).

The VC in the coronal plane was located on the medial side of the MPTG in 77.12% of patients, while the proportion of the online and lateral positions were 21.61% and 1.27%, respectively. There was no significant difference between males and females in this regard (*Table* 7).

Correlation analysis was conducted between measurements conforming to a normal distribution, and the correlation heatmap is shown in *Figure 10*. The angle between the VC and the sagittal plane and the angle between the SPF axis and the VC were slightly positively correlated. The angle between the VC and the sagittal plane and the angle between

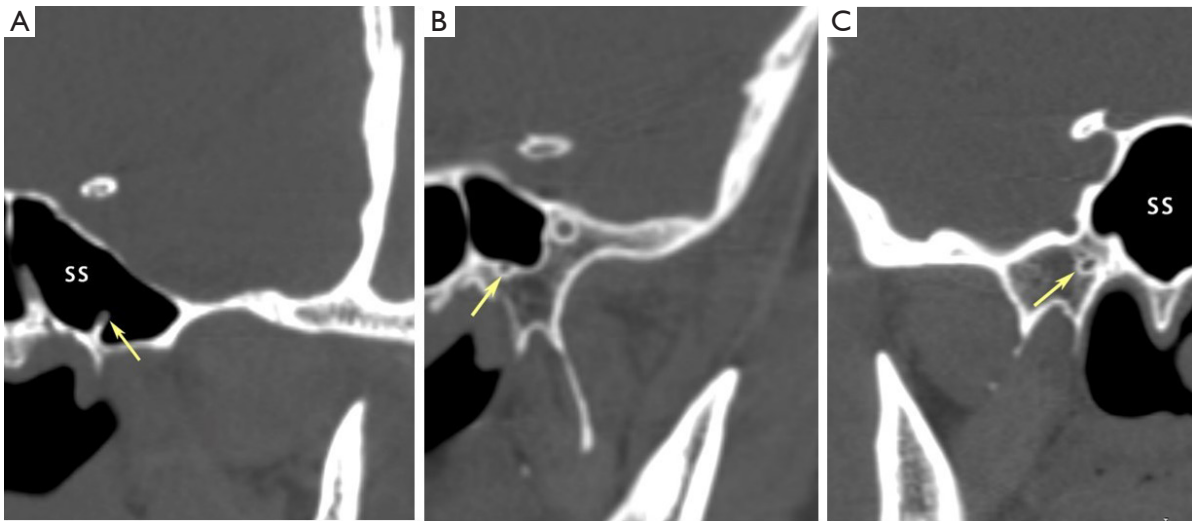

Figure 7 Coronal slices of the type 1 (A), type 2 (B), and type 3 (C) VC (yellow arrow). SS, sphenoid sinus; VC, vidian canal.

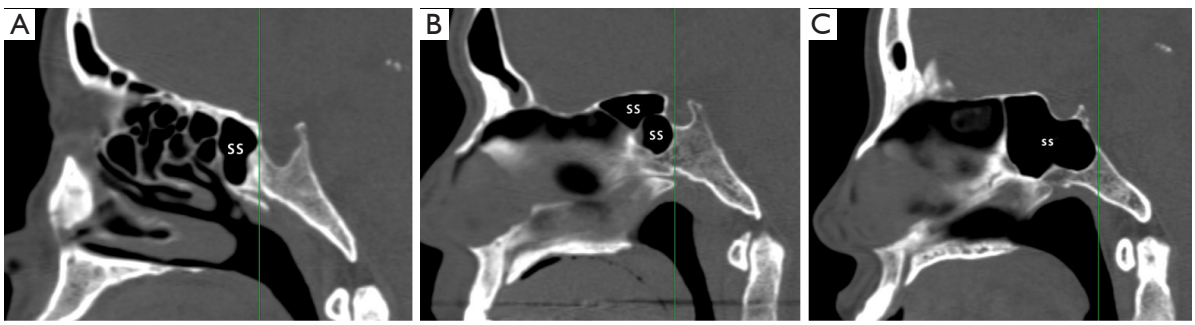

Figure 8 The sagittal slices with a straight line drawn along the posterior wall of the sphenoid sinus showing SS (A) type II (presellar), (B) type III (sellar), and (C) type IV (postsellar). SS, sphenoid sinus.

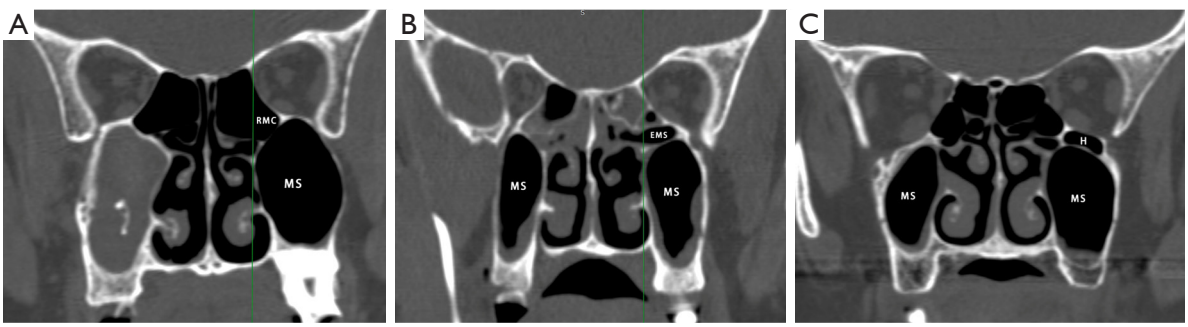

Figure 9 Coronal slices with a straight line drawn along the medial wall of the MS and the variation of the posterior ethmoid cells being identified as RMC (A), EMS (B), or Haller cells (C). RMC, retromaxillary air cell; MS, maxillary sinus; EMS, ethmomaxillary sinus; H, Haller cell.

Table 1 Demographic characteristics of patients included in the study

Age, years	Gender	N (%)	Total (%)
20 and under	Male	11 (9.32)	15 (12.71)
	Female	4 (3.39)	
21–30	Male	12 (10.17)	28 (23.73)
	Female	16 (13.56)	
31–40	Male	15 (12.71)	25 (21.19)
	Female	10 (8.47)	
41–50	Male	8 (6.78)	18 (15.25)
	Female	10 (8.47)	
51–60	Male	5 (4.24)	22 (18.64)
	Female	17 (14.41)	
61 and above	Male	4 (3.39)	10 (8.47)
	Female	6 (5.08)	

the VC and the PVC also indicated a slightly positive correlation. In addition, a slight positive correlation was found between the diameter of the SPF and the distance between the attachment of the end of the MT and the VC. The correlation of the distance between the SPF and the VC with the distance from the posterior wall of the MS to the VC were also slightly positive. We subjected the measurements with a of $P<0.05$ in correlation analysis to linear correlation analysis, and the regression coefficient and regression are shown in *Figure 10*.

A binary logistic regression analysis was conducted with the relative position between the pICA and the VC serving as the dependent variable. The results showed that sex, age, the angle between the VC and the sagittal plane, and the VC type were the related factors that might affect the

Table 2 Descriptive statistics and the results of the measurements for each gender

Item	Gender	N	Mean	SD	P value
Anterior diameter of the VC (mm)	Male	110	3.127	1.238	0.006
	Female	126	3.575	1.250	
Central diameter of the VC (mm)	Male	110	0.966	0.327	0.030
	Female	126	1.066	0.368	
Posterior diameter of the VC (mm)	Male	110	1.973	0.693	0.007
	Female	126	1.742	0.623	
Length of the VC (mm)	Male	110	14.000	3.351	0.001
	Female	126	12.513	3.420	
VC—sagittal angle plane (degree)	Male	110	14.139	5.988	0.000
	Female	126	17.449	5.369	
Diameter of the SPF (mm)	Male	110	4.916	1.887	0.524
	Female	126	5.069	1.794	
VC—SPF distance (mm)	Male	110	5.676	1.529	0.163
	Female	126	5.948	1.458	
VC—SPF angle (degree)	Male	110	143.107	8.798	0.044
	Female	126	145.683	10.713	
VC—end of MT distance (mm)	Male	110	7.276	4.153	0.000
	Female	126	9.471	4.182	
Posterior wall of MS—end of MT distance (mm)	Male	110	0.179	4.121	0.000
	Female	126	–1.767	4.186	
Posterior wall of MS—VC distance (mm)	Male	63	3.010	1.260	0.617
	Female	60	3.121	1.206	
PVC—VC angle (degree)	Male	110	62.505	16.780	0.182
	Female	126	65.303	15.317	
VC—FR distance (mm)	Male	110	6.479	2.580	0.020
	Female	126	5.761	2.135	

SD, standard deviation; VC, vidian canal; SPF, sphenopalatine foramen; MT, middle turbinate; MS, maxillary sinus; PVC, palatovaginal canal; FR, foramen rotundum.

Table 3 The ICC analysis of the measurements

Two-way mixed-effects single measures	ICC (C, 1)	95% CI
Anterior diameter of the VC	0.963	0.952–0.971
Central diameter of the VC	0.890	0.860–0.914
Posterior diameter of the VC	0.965	0.955–0.973
Length of the VC	0.987	0.983–0.990
VC—sagittal plane angle	0.987	0.984–0.990
Diameter of the SPF	0.981	0.975–0.985
VC—SPF distance	0.974	0.966–0.979
VC—SPF angle	0.943	0.927–0.956
VC—posterior wall of MS distance	0.965	0.954–0.972
VC—end of MT distance	0.994	0.992–0.995
PVC—VC angle	0.975	0.968–0.981
VC—FR distance	0.981	0.976–0.985

ICC, intraclass correlation coefficient; CI, confidence interval; VC, vidian canal; SPF, sphenopalatine foramen; MS, maxillary sinus; MT, middle turbinate; PVC, palatovaginal canal; FR, foramen rotundum.

Table 4 The prevalence of vidian canal types

Type	Male, n (%)	Female, n (%)	P value
Type 1	9 (3.81)	2 (0.85)	<0.001
Type 2	76 (32.20)	66 (27.97)	
Type 3	25 (10.59)	58 (24.58)	

Table 5 The prevalence of SS types

Type	Male, n (%)	Female, n (%)	P value
Type 1	0	0	0.137
Type 2	11 (4.66)	22 (9.32)	
Type 3	38 (16.10)	48 (20.34)	
Type 4	61 (25.85)	56 (23.73)	

SS, sphenoid sinus.

Table 6 The prevalence of ethmoid cell distribution

Variables	Male, n (%)	Female, n (%)	P value
None	2 (0.85)	10 (4.24)	0.189
RMC	90 (38.14)	94 (39.83)	
EMS	11 (4.66)	13 (5.51)	
Haller	7 (2.97)	9 (3.81)	

RMC, retromaxillary air cell; EMS, ethmomaxillary sinus.

Table 7 The prevalence of VC position according to different anatomical landmarks

Variable	Male, n (%)	Female, n (%)	P value
The medial wall of MS			0.144
Lateral	44 (18.64)	48 (20.34)	
Online	47 (19.92)	66 (27.97)	
Medial	19 (8.05)	12 (5.08)	
Palatovaginal canal			0.068
Superior	67 (28.39)	87 (36.86)	
Online	22 (9.32)	28 (11.86)	
Inferior	21 (8.90)	11 (4.66)	
pICA			0.028
Superior	0	0	
Online	32 (13.56)	54 (22.88)	
Inferior	78 (33.05)	72 (30.51)	
MPTG			0.378
Medial	81 (34.32)	101 (42.80)	
Online	28 (11.86)	23 (9.75)	
Lateral	1 (0.42)	2 (0.85)	

VC, vidian canal; MS, maxillary sinus; pICA, petrous internal carotid artery; MPTG, medial pterygoid plate.

anatomical relationship between the pICA and the VC (*Table 8*).

The results of the multinomial logistic regression analysis are shown in *Tables 9-14*. The dependent variables included the relative position between the medial wall of the MS and the VC in the axial plane, the position of the VC relative to the PVC in the coronal plane, the VC type, the position of the VC relative to the MPTG, and the classification of sphenoid sinus pneumatization.

Multiple linear regression analysis was conducted with the angle between VC and sagittal plane serving as the dependent variable, and multiple stepwise linear regression was determined. The results showed that the angle between the SPF and the VC, the transverse diameter of the anterior segment of the VC, and the relative relationship between the medial wall of MS and the VC might be the

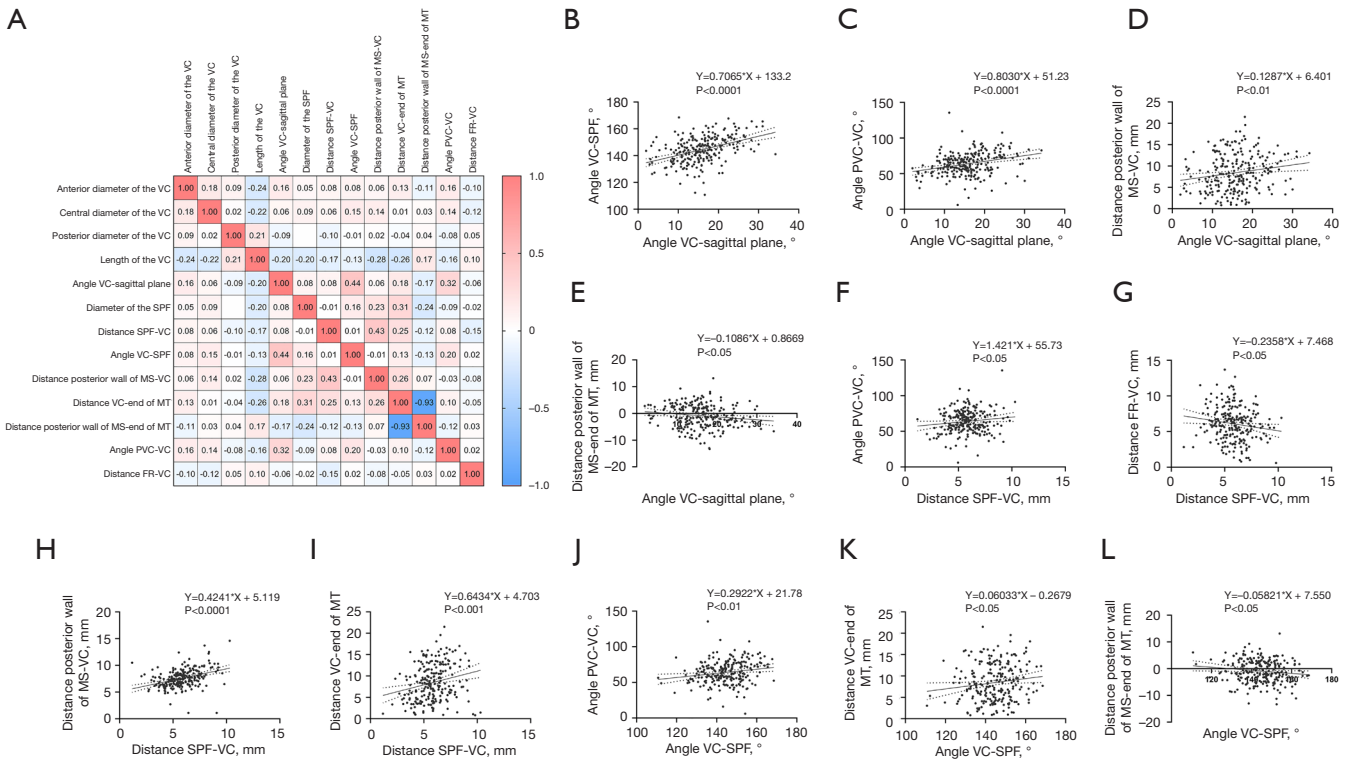

Figure 10 Correlation analysis of the measurements conforming to a normal distribution and simple linear regression analysis of the measurements with P<0.05 in the correlation analysis. (A) Correlation analysis of the anterior diameter of the VC, the central diameter of the VC, the posterior diameter of the VC, the length of the VC, the angle between the VC and the sagittal plane, the transverse diameter of the SPF, the distance from the VC to the SPF, the angle between the axis of the SPF and the VC, the distance from the posterior wall of the MS to the VC, the distance from the attachment of the end of the MT to the VC, the distance from the attachment of the end of the MT to the posterior wall of the MS (the distance from the posterior wall of the MS to the VC subtracted from the distance from the attachment of the end of the MT to the VC), the angle between the axis of the PVC and the VC, and the distance between the VC and the FR. The Spearman ρ value of each pair of terms is shown in the square grid. The red to blue bar in the right of the figure indicates the ρ value from 1.0 to −1.0. Blank boxes indicate that the P value of the correlation analysis between the 2 terms was greater than 0.05 and that the ρ value could not thus be obtained. (B) Linear correlation of the angle between the VC and the sagittal plane and the angle between the axis of the SPF and the VC. (C) Linear correlation of the angle between the VC and the sagittal plane and the angle between the axis of the PVC and the VC. (D) Linear correlation of the angle between the VC and the distance from the posterior wall of the MS to the VC. (E) Linear correlation of the distance from the attachment of the end of the MT to the posterior wall of the MS. (F) Linear correlation of the distance from the VC to the SPF and the axis of the PVC and the VC. (G) Linear correlation of the distance from the VC to the SPF and the distance between the VC and the FR. (H) Linear correlation of the distance from the VC to the SPF and the distance from the posterior wall of the MS to the VC. (I) Linear correlation of the distance from the VC to the SPF and the distance from the attachment of the end of the MT to the VC. (J) Linear correlation of the angle between the axis of the SPF and the VC and the angle between the axis of the PVC and the VC. (K) Linear correlation of the angle between the axis of the SPF and the VC and the distance from the attachment of the end of the MT to the VC. (L) Linear correlation of the angle between the axis of the SPF and the VC and the distance from the attachment of the end of the MT to the posterior wall of the MS. VC, vidian canal; SPF, sphenopalatine foramen; MS, maxillary sinus; MT, middle turbinate; PVC, palatovaginal canal; FR, foramen rotundum.

Table 8 Binary logic regression of the relative position between the VC and pICA

Variable	B	Exp(B)	95% CI	P value
Male	1.614	5.025	1.156–21.842	0.031
Age	–0.077	0.926	0.884–0.969	0.001
Lateral, left	0.732	2.079	0.534–8.090	0.291
Anterior diameter of the VC (mm)	0.293	1.340	0.815–2.203	0.249
Central diameter of the VC (mm)	0.002	1.002	0.194–5.181	0.998
Posterior diameter of the VC (mm)	0.649	1.913	0.720–5.082	0.193
Length of the VC (mm)	–0.074	0.929	0.786–1.097	0.384
VC—sagittal plane angle (degree)	–0.130	0.878	0.780–0.989	0.032
Diameter of the SPF (mm)	0.032	1.033	0.729–1.462	0.857
Distance VC—SPF (mm)	0.136	1.146	0.794–1.653	0.467
VC—SPF angle (degree)	0.067	1.069	0.991–1.153	0.082
Posterior wall of MS—end of MT distance (mm)	–0.012	0.988	0.712–1.273	0.942
VC—end of MT distance (mm)	0.126	1.135	0.968–1.330	0.119
Relative position of the medial wall of MS to VC	–0.969	0.380	0.079–1.816	0.225
PVC—VC angle (degree)	–0.004	0.996	0.960–1.033	0.835
Relative position the PVC to VC				0.332
Lateral	–1.056	0.348	0.045–2.662	0.309
Online	–0.049	0.952	0.112–8.061	0.964
VC type				0.017
Type 1	–3.594	0.027	0.002–0.484	0.014
Type 2	–1.989	0.137	0.029–0.639	0.011
VC-FR distance (mm)	0.243	1.275	0.967–1.680	0.085
SS type				0.481
Type 2	1.071	2.918	0.452–18.852	0.261
Type 3	0.432	1.541	0.439–5.412	0.500
Relative position the pICA to VC				0.167
Medial	23.133	11,132,360,778.464	0.000	0.999
Online	21.810	2,965,986,447.712	0.000	0.999
Type of infraorbital cells				0.352
RMC	2.640	14.016	0.675–291.190	0.088
EMS	0.824	2.279	0.268–19.386	0.451
Haller	1.402	4.061	0.113–146.128	0.443
(Constant)	–29.602			

VC, vidian canal; pICA, petrous internal carotid artery; CI, confidence interval; SPF, sphenopalatine foramen; MS, maxillary sinus; MT, middle turbinate; PVC, palatovaginal canal; FR, foramen rotundum; SS, sphenoid sinus; RMC, retromaxillary air cell; EMS, ethmomaxillary sinus.

Table 9 Multiple logic regression of the relative position between the VC and the medial wall of the MS

Location	Variable	B	Exp(B)	95% CI	P value
Medial[a]	Intercept	19.705			0.000
	Age	–0.015	0.985	0.962–1.009	0.216
	Anterior diameter of the VC (mm)	0.175	1.191	0.919–1.544	0.187
	Central diameter of the VC (mm)	–0.147	0.863	0.348–2.139	0.750
	Posterior diameter of the VC (mm)	0.150	1.162	0.716–1.885	0.543
	Length of the VC (mm)	–0.018	0.982	0.898–1.074	0.691
	VC—sagittal plane angle (degree)	0.032	1.033	0.967–1.103	0.333
	Diameter of the SPF (mm)	0.126	1.135	0.946–1.361	0.174
	VC—SPF distance (mm)	0.081	1.084	0.856–1.374	0.503
	VC—SPF angle (degree)	–0.010	0.990	0.953–1.029	0.608
	Posterior wall of MS—VC distance (mm)	–0.206	0.814	0.654–1.014	0.066
	VC—end of MT (mm) distance (mm)	–0.036	0.965	0.888–1.048	0.393
	PVC—VC angle (degree)	–0.005	0.995	0.974–1.015	0.611
	VC—FR distance (mm)	–0.025	0.976	0.838–1.136	0.750
	Male	0.249	1.283	0.663–2.599	0.489
	Female	0[b]			
	Lateral, left	0.444	1.560	0.788–3.088	0.202
	Lateral, right	0[b]			
	PVC lateral to VC	0.082	1.086	0.409–2.882	0.869
	PVC online with VC	–0.085	0.919	0.297–2.842	0.883
	PVC medial to VC	0[b]			
	Type 1 VC	–0.330	0.719	0.145–3.571	0.687
	Type 2 VC	–0.218	0.804	0.375–1.721	0.574
	Type 3 VC	0[b]			
	Type 2 SS	0.209	1.233	0.473–3.214	0.669
	Type 3 SS	–0.226	0.797	0.404–1.574	0.514
	Type 4 SS	0[b]			
	pICA superior to VC	–0.432	0.649	0.321–1.312	0.229
	pICA online with VC	0[b]			
	No infraorbital cells	0.408	1.505	0.248–9.117	0.657
	RMC infraorbital cells	–0.017	0.984	0.288–3.364	0.979
	EMS infraorbital cells	–1.006	0.366	0.072–1.867	0.226
	Haller infraorbital cells	0[b]			

Table 9 (*continued*)

Table 9 (*continued*)

Location	Variable	B	Exp(B)	95% CI	P value
Lateral[a]	Intercept	−5.560			0.286
	Age	0.044	1.046	1.007–1.086	0.022
	Anterior diameter of the VC (mm)	0.474	1.606	0.980–2.633	0.060
	Central diameter of the VC (mm)	−0.230	0.795	0.158–3.991	0.780
	Posterior diameter of the VC (mm)	−0.785	0.456	0.195–1.070	0.071
	Length of the VC (mm)	0.026	1.026	0.880–1.197	0.742
	VC—sagittal plane angle (degree)	−0.134	0.875	0.778–0.983	0.024
	Diameter of the SPF (mm)	0.101	1.106	0.831–1.472	0.489
	VC—SPF distance (mm)	−0.036	0.964	0.678–1.371	0.840
	VC—SPF angle (degree)	0.035	1.036	0.970–1.106	0.295
	Posterior wall of MS—VC distance (mm)	0.482	1.620	1.115–2.353	0.011
	VC—end of MT distance (mm)	−0.103	0.902	0.784–1.038	0.152
		0[b]			
	PVC—VC angle (degree)	−0.045	0.956	0.921–0.992	0.018
	VC—FR distance (mm)	−0.140	0.870	0.663–1.141	0.313
	Male	0.565	1.760	0.537–5.772	0.351
	Female	0[b]			
	Lateral, left	2.140	8.499	2.426–29.769	0.001
	Lateral, right	0[b]			
	PVC lateral to VC	−0.525	0.592	0.121–2.889	0.517
	PVC online with VC	−0.985	0.373	0.067–2.084	0.261
	PVC medial to VC	0[b]			
	Type 1 VC	−0.084	0.919	0.044–19.233	0.957
	Type 2 VC	0.328	1.389	0.382–5.045	0.618
	Type 3 VC	0[b]			
	Type 2 SS	−0.647	0.524	0.088–3.127	0.478
	Type 3 SS	−0.454	0.635	0.212–1.902	0.417
	Type 4 SS	0[b]			
	pICA superior to VC	−1.335	0.263	0.071–0.974	0.046
	pICA online with VC	0[b]			
	No infraorbital cells	−1.447	0.235	0.005–11.503	0.466
	RMC infraorbital cells	−0.229	0.796	0.068–9.262	0.855
	EMS infraorbital cells	−0.787	0.455	0.027–7.568	0.583
	Haller infraorbital cells	0[b]			

[a], the online type is used as the reference; [b], the constant is set to 0 because it is set as comparison. VC, vidian canal; MS, maxillary sinus; CI, confidence interval; SPF, sphenopalatine foramen; MT, middle turbinate; FR, foramen rotundum; PVC, palatovaginal canal; SS, sphenoid sinus; pICA, petrous internal carotid artery; RMC, retromaxillary air cell; EMS, ethmomaxillary sinus.

Table 10 Multiple logic regression of the relative position of the VC and the PVC

Location	Variable	B	Exp(B)	95% CI	P value
Superior[a]	Intercept	1.588			0.679
	Age	0.001	1.001	0.973–1.029	0.959
	Anterior diameter of the VC (mm)	–0.263	0.768	0.561–1.052	0.100
	Central diameter of the VC (mm)	1.129	3.093	0.846–11.310	0.088
	Posterior diameter of the VC (mm)	1.032	2.807	1.393–5.658	0.004
	Length of the VC (mm)	0.033	1.034	0.927–1.153	0.554
	VC—sagittal plane angle (degree)	0.017	1.017	0.941–1.099	0.665
	Diameter of the SPF (mm)	0.123	1.131	0.904–1.416	0.282
	VC—SPF distance (mm)	–0.155	0.857	0.644–1.139	0.288
	VC—SPF angle (degree)	–0.045	0.956	0.913–1.000	0.052
	Posterior wall of MS—VC distance (mm)	0.082	1.085	0.854–1.379	0.504
	VC—end of MT distance (mm)	0.038	1.039	0.938–1.151	0.464
	Posterior wall of MS—end of MT distance (mm)	0[b]			
	PVC—VC angle (degree)	0.013	1.014	0.988–1.040	0.307
	VC—FR distance (mm)	0.025	1.025	0.850–1.236	0.795
	Male	–0.194	0.823	0.353–1.922	0.653
	Female	0[b]			
	Lateral, left	–0.743	0.476	0.203–1.115	0.087
	Lateral, right	0[b]			
	VC lateral to the medial wall of MS	–0.017	0.983	0.272–3.551	0.979
	VC online with the medial wall of MS	–0.050	0.951	0.284–3.191	0.936
	VC medial to the medial wall of MS	0[b]			
	Type 2 SS	–0.127	0.880	0.269–2.887	0.834
	Type 3 SS	0.289	1.335	0.564–3.163	0.511
	Type 4 SS	0[b]			
	pICA superior to VC	0.365	1.441	0.605–3.433	0.410
	pICA online with VC	0[b]			
	VC medial to MPTG	2.712	15.066	0.745–304.859	0.077
	VC online with MPTG	2.937	18.853	0.894–397.481	0.059
	VC lateral to MPTG	0[b]			
	No infraorbital cells	–0.934	0.393	0.046–3.392	0.396
	RMC infraorbital cells	0.060	1.062	0.205–5.516	0.943
	EMS infraorbital cells	–0.333	0.717	0.100–5.143	0.741
	Haller infraorbital cells	0[b]			

Table 10 (*continued*)

Table 10 (*continued*)

Location	Variable	B	Exp(B)	95% CI	P value
Inferior[b]	Intercept	−9.359			0.117
	Age	0.023	1.023	0.979–1.069	0.313
	Anterior diameter of the VC (mm)	−0.884	0.413	0.233–0.732	0.002
	Central diameter of the VC (mm)	−0.764	0.466	0.050–4.337	0.502
	Posterior diameter of the VC (mm)	0.430	1.537	0.571–4.132	0.395
	Length of the VC (mm)	0.083	1.086	0.925–1.276	0.312
	VC—sagittal plane angle (degree)	0.132	1.141	1.017–1.280	0.024
	Diameter of the SPF (mm)	0.081	1.084	0.775–1.516	0.637
	VC—SPF distance (mm)	−0.276	0.759	0.518–1.112	0.157
	VC—SPF angle (degree)	−0.104	0.901	0.835–0.972	0.007
	Posterior wall of MS—VC distance (mm)	0.311	1.365	0.938–1.987	0.104
	VC—end of MT distance (mm)	−0.257	0.773	0.645–0.927	0.005
	Posterior wall of MS—end of MT distance (mm)	0[b]			
	PVC—VC angle (degree)	0.025	1.025	0.987–1.064	0.195
	VC—FR distance (mm)	0.188	1.207	0.934–1.559	0.150
	Male	−0.019	0.981	0.262–3.670	0.978
	Female	0[b]			
	Lateral, left	−0.896	0.408	0.115–1.449	0.166
	Lateral, right	0[b]			
	VC lateral to the medial wall of MS	0.104	1.110	0.194–6.354	0.907
	VC online with the medial wall of MS	−0.133	0.876	0.170–4.499	0.874
	VC medial to the medial wall of MS	0[b]			
	Type 2 SS	0.325	1.383	0.208–9.214	0.737
	Type 3 SS	1.293	3.645	1.071–12.401	0.038
	Type 4 SS	0[b]			
	pICA superior to VC	0.169	1.185	0.319–4.406	0.800
	pICA online with VC	0[b]			
	VC medial to MPTG	18.992	176,995,448.173	37,414,503.680–837,306,006.819	0.000
	VC online with MPTG	19.018	181,747,877.515	181,747,877.514–181,747,877.515	
	VC lateral to MPTG	0[b]			
	No infraorbital cells	0.434	1.543	0.055–43.043	0.798
	RMC infraorbital cells	1.114	3.048	0.250–37.134	0.382
	EMS infraorbital cells	1.778	5.917	0.289–121.121	0.248
	Haller infraorbital cells	0[b]			

[a], the online type is used as the reference; [b], the constant is set to 0 because it is set as comparison. VC, vidian canal; PVC, palatovaginal canal; SPF, sphenopalatine foramen; MS, maxillary sinus; MT, middle turbinate; FR, foramen rotundum; SS, sphenoid sinus; MPTG, medial pterygoid plate; RMC, retromaxillary air cell; EMS, ethmomaxillary sinus.

Table 11 Multiple logic regression of the VC type

Type 2[a]	B	Exp(B)	95% CI	P value
Intercept	–17.735			0.009
Age	–0.022	0.978	0.932–1.027	0.378
Anterior diameter of the VC (mm)	0.422	1.525	0.924–2.518	0.099
Central diameter of the VC (mm)	–1.090	0.336	0.071–1.544	0.161
Posterior diameter of the VC (mm)	1.071	2.918	1.056–8.060	0.039
Length of the VC (mm)	0.058	1.059	0.919–1.221	0.427
VC—sagittal plane angle (mm)	–0.071	0.932	0.809–1.072	0.327
Diameter of the SPF (mm)	0.213	1.237	0.857–1.785	0.256
VC—SPF distance (mm)	0.215	1.240	0.838–1.836	0.282
VC—SPF angle (degree)	0.069	1.072	0.987–1.163	0.098
VC—end of MT distance(mm)	–0.034	0.966	0.665–1.404	0.858
Posterior wall of MS—end of MT distance (mm)	0.001	1.001	0.719–1.393	0.996
Posterior wall of MS—VC distance (mm)	–0.190	0.827	0.489–1.396	0.477
PVC—VC angle (degree)	–0.034	0.967	0.931–1.004	0.077
VC—FR distance (mm)	0.577	1.781	1.313–2.414	0.000
Male	1.703	5.490	1.454–20.726	0.012
Female	0[b]			
Lateral, left	1.090	2.975	0.691–12.804	0.143
Lateral, right	0[b]			
VC lateral to the medial wall of MS	–0.289	0.749	0.171–3.278	0.701
VC medial to the wall of MS	0[b]			
PVC lateral to VC	–0.038	0.963	0.154–6.034	0.968
PVC online with VC	1.657	5.244	0.641–42.923	0.122
PVC medial to VC	0[b]			
Type 2 SS	0.265	1.303	0.236–7.207	0.762
Type 3 SS	0.158	1.172	0.288–4.764	0.825
Type 4 SS	0[b]			
PICA superior to VC	1.977	7.220	1.556–33.506	0.012
PICA online with VC	0[b]			
VC medial to MPTG	2.953	19.168	0.444–828.105	0.124
VC online with MPTG	1.229	3.418	0.082–142.371	0.518
VC lateral to MPTG	0[b]			
No infraorbital cells	3.795	44.492	1.048–1,888.916	0.047
No infraorbital cells	–0.289	0.749	0.070–7.960	0.811
RMC infraorbital cells	0.336	1.399	0.064–30.567	0.831
EMS infraorbital cells	0[b]			

[a], type 3 is used as the reference; [b], the constant is set to 0 because it is set as comparison. VC, vidian canal; CI, confidence interval; SPF, sphenopalatine foramen; MS, maxillary sinus; MT, middle turbinate; PVC, palatovaginal canal; FR, foramen rotundum; pICA, petrous internal carotid artery; MPTG, medial pterygoid plate; RMC, retromaxillary air cell; EMS, ethmomaxillary sinus.

Table 12 Multiple logic regression of the relative position between VC and the MPTG

Medial[a]	B	Exp(B)	95% CI	P value
Intercept	8.362			0.036
Age	–0.020	0.980	0.952–1.009	0.179
Anterior diameter of the VC (mm)	–0.384	0.681	0.502–0.923	0.013
Central diameter of the VC (mm)	–0.591	0.554	0.196–1.564	0.264
Posterior diameter of the VC (mm)	0.121	1.129	0.634–2.009	0.681
Length of the VC (mm)	–0.101	0.904	0.792–1.031	0.132
VC—sagittal plane angle (degree)	0.115	1.122	1.032–1.220	0.007
Diameter of the SPF (mm)	–0.029	0.971	0.773–1.220	0.803
VC—SPF distance (mm)	0.069	1.071	0.813–1.411	0.624
VC—SPF angle (degree)	–0.011	0.989	0.943–1.038	0.661
Posterior wall of MS—VC distance	–0.234	0.791	0.614–1.019	0.069
VC—end of MT distance(mm)	0.065	1.067	0.961–1.184	0.227
PVC—VC angle (degree)	–0.028	0.972	0.946–0.999	0.041
VC—FR distance (mm)	0.120	1.127	0.923–1.377	0.239
Male	–0.589	0.555	0.231–1.334	0.188
Female	0[b]			
Lateral, left	–1.163	0.313	0.126–0.777	0.012
Lateral, right	0[b]			
VC lateral to the medial wall of MS	–1.583	0.205	0.049–0.869	0.032
VC online with the medial wall of MS	–1.267	0.282	0.067–1.175	0.082
VC medial to the wall of MS	0[b]			
PVC lateral to VC	0.162	1.176	0.341–4.052	0.797
PVC online with VC	0.442	1.555	0.373–6.481	0.544
PVC medial to VC	0[b]			
Type 1 VC	–0.858	0.424	0.071–2.523	0.346
Type 2 VC	0.368	1.445	0.590–3.540	0.421
Type 3 VC	0[b]			
Type 2 SS	–0.762	0.467	0.151–1.446	0.187
Type 3 SS	0.118	1.125	0.480–2.638	0.787
Type 4 SS	0[b]			
PICA superior to VC	–0.536	0.585	0.254–1.348	0.208
PICA online with VC	0[b]			
No infraorbital cells	1.933	6.911	0.521–91.596	0.143
No infraorbital cells	0.700	2.014	0.469–8.644	0.346
RMC infraorbital cells	1.965	7.138	0.838–60.840	0.072
EMS infraorbital cells	0[b]			

[a], the online type is used as the reference; [b], the constant is set to 0 because it is set as comparison. VC, vidian canal; MPTG, medial pterygoid plate; CI, confidence interval; SPF, sphenopalatine foramen; MS, maxillary sinus; MT, middle turbinate; FR, foramen rotundum; PVC, palatovaginal canal; SS, sphenoid sinus; pICA, petrous internal carotid artery; RMC, retromaxillary air cell; EMS, ethmomaxillary sinus.

Table 13 Multiple logic regression of the SS type

Type	Variable	B	Exp(B)	95% CI	P value
Type 2[a]	Intercept	23.115			0.000
	Age	−0.007	0.993	0.959–1.027	0.692
	Anterior diameter of the VC (mm)	−0.481	0.618	0.401–0.951	0.029
	VC—sagittal plane angle (degree)	0.056	1.058	0.094–1.162	0.235
	VC—SPF distance (mm)	0.056	1.058	0.746–1.499	0.753
	VC—SPF angle (degree)	−0.012	0.988	0.937–1.042	0.660
	Posterior wall of MS—VC distance (mm)	−0.211	0.810	0.594–1.104	0.182
	VC—end of MT distance(mm)	0.073	1.076	0.961–1.205	0.205
	PVC—VC angle (degree)	−0.026	0.974	0.945–1.004	0.092
	VC—FR distance (mm)	−0.037	0.964	0.777–1.196	0.739
	Male	−0.608	0.545	0.191–1.553	0.256
	Female	0[b]			
	Lateral, left	0.256	1.292	0.476–3.351	0.615
	Lateral, right	0[b]			
	VC lateral to the medial wall of MS	0.161	1.174	0.240–5.744	0.843
	VC online with the medial wall of MS	−0.056	0.945	0.203–4.402	0.943
	VC medial to the wall of MS	0[b]			
	PVC lateral to VC	0.075	1.077	0.220–5.272	0.927
	PVC online with VC	0.272	1.313	0.225–7.663	0.762
	PVC medial to VC	0[b]			
	Type 1 VC	−0.565	0.568	0.070–4.584	0.596
	Type 2 VC	−1.142	0.319	0.110–0.928	0.036
	Type 3 VC	0[b]			
	VC medial to MPTG	−18.477	0.000	0.000–0.000	0.000
	VC online with MPTG	−17.694	0.000	0.000–0.000	0.000
	VC lateral to MPTG	0[b]			
	No infraorbital cells	−0.789	0.454	0.027–7.769	0.586
	No infraorbital cells	−0.662	0.516	0.094–2.825	0.445
	RMC infraorbital cells	0.914	2.493	0.301–20.667	0.397
	EMS infraorbital cells	0[b]			

Table 13 (*continued*)

Table 13 (*continued*)

Type	Variable	B	Exp(B)	95% CI	P value
Type 3[a]	Intercept	15.104			0.000
	Age	0.017	1.017	0.995–1.040	0.139
	Anterior diameter of the VC (mm)	−0.011	0.989	0.763–1.284	0.936
	VC—sagittal plane angle	−0.009	0.991	0.928–1.058	0.787
	VC—SPF distance (mm)	0.065	1.067	0.849–1.340	0.577
	VC—SPF angle (degree)	0.015	1.015	0.977–1.054	0.438
	Posterior wall of MS—VC distance (mm)	−0.054	0.948	0.771–1.165	0.610
	VC—end of MT distance(mm)	0.077	1.080	0.997–1.170	0.060
	PVC—VC angle (degree)	0.002	1.002	0.982–1.024	0.830
	VC—FR distance (mm)	−0.130	0.878	0.754–1.022	0.093
	Male	0.119	1.126	0.568–2.234	0.734
	Female	0[b]			
	Lateral, left	0.698	2.009	0.994–4.062	0.052
	Lateral, right	0[b]			
	VC lateral to the medial wall of MS	0.279	1.322	0.460–3.799	0.604
	VC online with the medial wall of MS	0.459	1.583	0.583–4.296	0.367
	VC medial to the wall of MS	0[b]			
	PVC lateral to VC	−1.012	0.364	0.139–0.952	0.039
	PVC online with VC	−1.088	0.337	0.110–1.030	0.056
	PVC medial to VC	0[b]			
	Type 1 VC	−1.584	0.205	0.020–2.054	0.178
	Type 2 VC	−0.390	0.677	0.325–1.408	0.296
	Type 3 VC	0[b]			
	VC medial to MPTG	−16.873	0.000	0.000–0.000	0.000
	VC online with MPTG	−16.964	0.000	0.000–0.000	
	VC lateral to MPTG	0[b]			
	No infraorbital cells	−0.803	0.448	0.072–2.772	0.388
	No infraorbital cells	−0.849	0.428	0.124–1.476	0.179
	RMC infraorbital cells	−0.104	0.901	0.185–4.396	0.898
	EMS infraorbital cells	0[b]			

[a], type 4 is used as the reference; [b], the constant is set to 0 because it is set as comparison. SS, sphenoid sinus; CI, confidence interval; VC, vidian canal; SPF, sphenopalatine foramen; MS, maxillary sinus; MT, middle turbinate; PVC, palatovaginal canal; FR, foramen rotundum; MPTG, medial pterygoid plate; RMC, retromaxillary air cell; EMS, ethmomaxillary sinus.

Table 14 Multiple logic regression of the anatomical variation of infraorbital cells

RMC[a]	B	Exp(B)	95% CI	P value
Intercept	39.379			0.997
Age	0.010	1.010	0.909–1.122	0.855
Anterior diameter of the VC (mm)	1.210	3.355	0.629–17.903	0.157
central diameter of the VC (mm)	0.678	1.970	0.027–145.951	0.757
Posterior diameter of the VC (mm)	–1.927	0.146	0.009–2.458	0.181
Length of the VC (mm)	–0.429	0.651	0.284–1.495	0.312
VC—sagittal plane angle	–0.130	0.878	0.677–1.139	0.328
Diameter of the SPF (mm)	–0.142	0.868	0.428–1.758	0.694
VC—SPF distance (mm)	0.085	1.088	0.438–2.705	0.855
VC—SPF angle (degree)	–0.050	0.951	0.759–1.192	0.664
Posterior wall of MS—VC distance (mm)	–0.103	0.902	0.374–2.175	0.819
VC—end of MT distance (mm)	–0.110	0.896	0.384–2.093	0.800
PVC—VC angle (degree)	–0.029	0.972	0.849–1.112	0.676
VC—FR distance (mm)	–0.352	0.703	0.325–1.520	0.371
Male	2.782	16.155	0.094–2,785.264	0.290
Female	0[b]			
Lateral, left	1.834	6.256	0.107–364.164	0.377
Lateral, right	0[b]			
VC lateral to the medial wall of MS	–1.563	0.210	0.001–37,729	0.555
VC medial to the wall of MS	0[b]			
Type 2 SS	3.146	23.246	0.012–45,164.810	0.415
Type 3 SS	–0.863	0.422	0.030–5.895	0.521
Type 4 SS	0[b]			
PICA superior to VC	–2.158	0.116	0.006–2.187	0.150
PICA online with VC	0[b]			
VC medial to MPTG	3.798	44.595	0.127–15,698.957	0.204
VC online with MPTG	3.915	50.136	0.057–43,904.416	0.257
VC lateral to MPTG	0[b]			

[a], the Haller cell type is used as the reference; [b], the constant is set to 0 because it is set as comparison. RMC, retromaxillary air cell; CI, confidence interval; VC, vidian canal; SPF, sphenopalatine foramen; MS, maxillary sinus; MT, middle turbinate; PVC, palatovaginal canal; FR, foramen rotundum; MPTG, medial pterygoid plate.

Table 15 Multiple linear regression analysis of the angle between the VC and the sagittal plane

Variable	B	Standard error	β	P value
(Constant)	−20.265	8.616		0.021
Gender	0.654	1.089	0.058	0.550
Age	−0.034	0.038	−0.080	0.381
Lateral	−3.066	1.045	−0.271	0.004
Anterior diameter of the VC (mm)	1.094	0.383	0.258	0.005
Central diameter of the VC (mm)	−1.780	1.309	−0.117	0.177
Posterior diameter of the VC (mm)	−0.454	0.726	−0.053	0.533
Length of the VC (mm)	0.086	0.127	0.057	0.498
Diameter of the SPF (mm)	−0.001	0.267	0.000	0.998
VC—SPF distance (mm)	0.220	0.322	0.060	0.495
VC—SPF angle (degree)	0.270	0.056	0.448	0.000
VC—end of MT distance (mm)	0.193	0.288	0.156	0.503
Posterior wall of MS—end of MT distance (mm)	0.096	0.270	0.078	0.722
Relative position the medial wall of MS to VC	−1.462	0.590	−0.226	0.015
PVC—VC angle (degree)	0.015	0.030	0.045	0.613
Relative position the PVC to VC	0.851	0.645	0.110	0.190
VC type	0.358	0.970	0.035	0.713
VC—FR distance (mm)	−0.177	0.213	−0.074	0.406
SS type	−0.093	0.640	−0.012	0.885
Relative position of pICA to VC	−2.221	1.075	−0.185	0.041
Relative position of MPTG to VC	−1.611	1.008	−0.142	0.113
Presence of infraorbital cells	−0.734	2.135	−0.030	0.732

VC, vidian canal; SPF, sphenopalatine foramen; MT, middle turbinate; MS, maxillary sinus; PVC, palatovaginal canal; FR, foramen rotundum; SS, sphenoid sinus; MPTG, medial pterygoid plate.

independent risk factors for the angle between VC and the sagittal plane (*Table 15*).

Discussion

The use of CT may contribute to the preoperative evaluation of VN according to the position and morphometric information of the VC. We found that the transverse diameter and the length of the VC vary between the females and males. The VC was inferior to the internal carotid artery (ICA) in most cases, and some of the measurements of the VC and its surrounding structures were correlated. Endoscopic VN (EVN), a surgical therapy for AR and VMR, plays a key role in the treatment of severe persistent AR (7,9). However, the anterior opening of the VC is narrow, and the anatomical structure around it is complex. In addition, there are important blood vessels and nerves in the PPF. Identifying the fine anatomy of the VC and its surrounding structures is an important prerequisite for EVN in the treatment of AR. Understanding the relationship between the adjacent structures of the VC and their anatomical variation is of great value for preoperative risk assessment and intraoperative navigation. One of the common approaches for the vidian nerve is curving an incision along the posterior edge of the MT and finding the SPF (12,18), and the other is exposing the VC through the sphenoidal sinus (19,20). In this study, based on previous research on the VC and considering the surgical

approaching and protecting of blood vessels and nerves in VN, we observed and measured a certain series of values.

In this study, the average length of the VC in male and female patients was 14.00±3.35 and 12.51±3.42 mm, respectively, which was in line with the report by Vuksanovic-Bozaric *et al.* (15) and Wang *et al.* (21). Among the 118 patients, the transverse diameter of the posterior segment of the VC in females was larger than that in males, and the length of the VC and the distance between VC and FR in males were longer than those in females. The angle between the VC and the sagittal plane and the angle between the SPF and the VC in females were larger than those in males, and the distance between the attachment to the end of the MT and the VC was greater. This may suggest that the VC of females is shorter, thicker, and flatter than that of males.

The relative relationship between the anterior opening of the VC and the medial wall of the MS was reported for the first time in this study. This may serve as a reference in the evaluation of operative risk and difficulty, as the position of the medial wall of the MS may affect the degree of difficulty of intraoperative operation when the vidian nerve is approached through the middle nasal meatus.

The shortest distance between the VC and the FR in the coronal plane was 6.48±2.58 mm in males and 5.76±2.13 mm in females, which was also consistent with previous reports (15,22,23). The protection of the maxillary nerve is critical, and great care should be taken when EVN is being conducted. Unfortunately, the linear regression analysis did not identify any related factors, possibly due to the multicollinearity of the indicators included or the limited sample size. Increasing the sample size and conducting stepwise regression can be implemented in future research to more definitively verify the reliability of our conclusions.

Observed in the coronal plane, the highest point of the PVC was higher than the VC, but the opposite situation was found in a few patients. The identification of the PVC and its relative position with the VC is crucial to locating and identifying the VC during VN, as this can facilitate intraoperative navigation and rapid location of the anterior opening of the VC.

In the correlation analysis, the transverse diameter of the SPF and the distance from the attachment of the end of the MT to the VC showed a slightly positive correlation, indicating that the larger the SPF is, the longer the distance between the end of the MT and the VC. An approach to the vidian nerve through the middle nasal meatus provides more space for a safe operation in those with a small SPF, meaning the measurement of SPF may have value as a reference for surgical risk assessment.

The distance between the SPF and the VC and the distance from the posterior wall of the MS to the VC showed a slightly positive correlation. These two measurements were related to the distance from the MT to the VC through the middle nasal meatus in the operation. This may contribute to the surgical risk assessment in the preoperative evaluation of patients who opt for this surgical approach, but its clinical significance should be researched further and confirmed.

The VN operation via the sphenoid sinus can vary according to the classification of the VC (24). Among the patients included in this study, the most common VC type was type 2, which is consistent with other reports (6,24-26). The results of logistic regression analysis indicated type 2 VC was more likely to occur in males with a larger transverse diameter of the posterior segment of the VC, those with longer distance from the VC to the FR, those with the pICA located in the same line with VC, and those without infraorbital cells. Some patients with type 3 VC need removal of part of the sphenoid process of the palatine bone and even part of the ethmoid bone for the VC to be identified, and this should be taken into account in the selection of the sphenoid sinus approach in VN. We suggest that the abovementioned anatomical values should be carefully considered in the selection of the surgical approach and the evaluation of surgical trauma.

Regarding the type of sphenoid sinus pneumatization, type 3 predominated among our patients. Logistic regression analysis suggested that patients with a smaller transverse diameter of the posterior segment of VC, non-type 2 VC, and an MPTG located laterally to the VC were more likely to be type 2 sphenoid sinus pneumatization. Patients with a PVC above the VC and an MPTG located on the lateral side of the VC were more likely to be type 3. In conducting a VN via the sphenoid sinus, the pneumatization of SS may intraoperatively provide a safer operative space.

Among the 118 patients included in the study, logistic regression analysis indicated that the terminal aspect of the VC being inferior to the level of the pICA was more likely to occur in females, younger patients, and those with a smaller angle between the VC and the sagittal plane. In type 1 VC or type 2 VC patients, the terminal aspect of VC was more likely to be inferior to the pICA compared to those with type 3. Notably, although the VC is often regarded as an anatomical site of surgery related to the

PPF in clinical practice for protecting the ICA (22,27,28), some studies (22,27) have reported that the pICA is located superior to the terminal aspect of the VC in a few cases. This measurement should be thoroughly considered during preoperative evaluation in order to avoid injury to the pICA and severe intraoperative bleeding.

Although we confirmed that CT can provide valuable anatomical reference information for VN, there are some limitations to our study that should be mentioned. First, in order to verify the significance of CT assessment during VN in surgical practice, a cohort study to assess the method in this study among patients who have undergone VN should be conducted. In addition, the observational study in patients with AR or a study grouped according to whether the patients have been diagnosed with AR could be conducted to confirm the generalizability of our findings.

In summary, CT may contribute to the preoperative evaluation of VN according to the position and morphometric information of the VC. Moreover, our findings may also serve as a valuable reference for other types of paranasal surgery. The anatomical characteristics of the surrounding structures of the VC and paranasal sinuses could also be clarified in a preoperative CT scan. This would help locate structures, such as the PPF and FR, which could contribute to successfully implementing related extensive surgical techniques, such as centripetal sinus surgery (29). In the preoperative evaluation of surgery, CT can be used to initially inform the selection of surgical preoperative treatment for patients with AR, improve risk assessment, and thus enhance patient care. Real-time evaluation of patients of AR according to gender can also be performed during and after surgery to help evaluate the treatment effect.

Conclusions

The anatomical structure of VC under CT varies according to gender. VN can be evaluated preoperatively according to the location and morphological information of the VC. Depending on the variation of the VC's surrounding structure, CT may be beneficial for preoperative planning, intraoperative evaluation, and postoperative care. This study is the first to report on the differences between the location and morphology of VC on CT between genders. Despite the innate limitations of retrospective studies, we believe our study demonstrates that carefully evaluating the anatomical structure of VC provides indispensable advantages and has potential for further clinical application preoperatively and postoperatively.

Acknowledgments

We thank Dr. Nayellin Reyes-Chicuellar (Royal Darwin Hospital, Darwin, Australia) for providing critical commentary and valuable advice concerning this study.
Funding: None.

Footnote

Reporting Checklist: The authors have completed the STROBE reporting checklist. Available at https://qims.amegroups.com/article/view/10.21037/qims-23-1033/rc

Conflicts of Interest: All authors have completed the ICMJE uniform disclosure form (available at https://qims.amegroups.com/article/view/10.21037/qims-23-1033/coif). The authors have no conflicts of interest to declare.

Ethical Statement: The authors are accountable for all aspects of the work in ensuring that questions related to the accuracy or integrity of any part of the work are appropriately investigated and resolved. The study was conducted in accordance with the Declaration of Helsinki (as revised in 2013) and was approved by the Ethics Committee of Renmin Hospital of Wuhan University (No. WDRY2022-K237). The requirement for informed consent in this study was waived due to its retrospective nature.

References

1. Brożek JL, Bousquet J, Agache I, Agarwal A, Bachert C, Bosnic-Anticevich S, et al. Allergic Rhinitis and its Impact on Asthma (ARIA) guidelines-2016 revision. J Allergy Clin Immunol 2017;140:950-8.
2. Schuler Iv CF, Montejo JM. Allergic Rhinitis in Children and Adolescents. Immunol Allergy Clin North Am

2021;41:613-25.
3. Zhang Y, Lan F, Zhang L. Advances and highlights in allergic rhinitis. Allergy 2021;76:3383-9.
4. Nur Husna SM, Tan HT, Md Shukri N, Mohd Ashari NS, Wong KK. Allergic Rhinitis: A Clinical and Pathophysiological Overview. Front Med (Lausanne) 2022;9:874114.
5. Dierick BJH, van der Molen T, Flokstra-de Blok BMJ, Muraro A, Postma MJ, Kocks JWH, van Boven JFM. Burden and socioeconomics of asthma, allergic rhinitis, atopic dermatitis and food allergy. Expert Rev Pharmacoecon Outcomes Res 2020;20:437-53.
6. Rahmati A, Ghafari R, AnjomShoa M. Normal Variations of Sphenoid Sinus and the Adjacent Structures Detected in Cone Beam Computed Tomography. J Dent (Shiraz) 2016;17:32-7.
7. Okubo K, Kurono Y, Ichimura K, Enomoto T, Okamoto Y, Kawauchi H, Suzaki H, Fujieda S, Masuyama K; . Japanese guidelines for allergic rhinitis 2020. Allergol Int 2020;69:331-45.
8. Scadding GK, Kariyawasam HH, Scadding G, Mirakian R, Buckley RJ, Dixon T, Durham SR, Farooque S, Jones N, Leech S, Nasser SM, Powell R, Roberts G, Rotiroti G, Simpson A, Smith H, Clark AT. BSACI guideline for the diagnosis and management of allergic and non-allergic rhinitis (Revised Edition 2017; First edition 2007). Clin Exp Allergy 2017;47:856-89.
9. Yan CH, Hwang PH. Surgical Management of Nonallergic Rhinitis. Otolaryngol Clin North Am 2018;51:945-55.
10. Ai J, Xie Z, Qing X, Li W, Liu H, Wang T, Tan G. Clinical Effect of Endoscopic Vidian Neurectomy on Bronchial Asthma Outcomes in Patients with Coexisting Refractory Allergic Rhinitis and Asthma. Am J Rhinol Allergy 2018;32:139-46.
11. Wu AW, Ting JY. Indications for surgery in refractory rhinitis. Curr Allergy Asthma Rep 2014;14:414.
12. Tan G, Ma Y, Li H, Li W, Wang J. Long-term results of bilateral endoscopic vidian neurectomy in the management of moderate to severe persistent allergic rhinitis. Arch Otolaryngol Head Neck Surg 2012;138:492-7.
13. Krajina Z. Critical review of Vidian neurectomy. Rhinology 1989;27:271-6.
14. Açar G, Çiçekcibaşı AE, Çukurova İ, Özen KE, Şeker M, Güler İ. The anatomic analysis of the vidian canal and the surrounding structures concerning vidian neurectomy using computed tomography scans. Braz J Otorhinolaryngol 2019;85:136-43.
15. Vuksanovic-Bozaric A, Vukcevic B, Abramovic M, Vukcevic N, Popovic N, Radunovic M. The pterygopalatine fossa: morphometric CT study with clinical implications. Surg Radiol Anat 2019;41:161-8.
16. Zhou F, Cao C, Fan W, Tan L, Liu P, Lv H, Xu Y. The imaging anatomy of ethmomaxillary sinus and its impact on chronic rhinosinusitis. Eur Arch Otorhinolaryngol 2021;278:719-26.
17. Cao C, Zhou F, Song Z, Tao Z, Xu Y. Computed Tomography Image Analysis and Clinical Correlations of Retromaxillary Cells. Ear Nose Throat J 2022;101:435-42.
18. Shen L, Wang J, Kang X, Han M, Li M, Huang Z, Luo L, Tu J, Ye J. Clinical Efficacy and Possible Mechanism of Endoscopic Vidian Neurectomy for House Dust Mite-Sensitive Allergic Rhinitis. ORL J Otorhinolaryngol Relat Spec 2021;83:75-84.
19. Ahilasamy N, Rajendran Dinesh K. Endoscopic posterior nasal neurectomy. J Laryngol Otol 2019;133:825-9.
20. Zhao C, Ji Y, An Y, Xue J, Li Q, Suo L, Hou R, Zhang Y, Geng Z, Shen H, Ren J, Yang P. An Alternative Method of Endoscopic Intrasphenoidal Vidian Neurectomy. OTO Open 2018;2:2473974X18764862.
21. Wang X, Yu H, Cai Z, Wang Z, Ma B, Zhang Y, Ye Z. Anatomical study on Meckel cave with endoscopic endonasal, endo-maxillary sinus, and endo-pterygoid process approaches. PLoS One 2014;9:e91444.
22. Papavasileiou G, Hajiioannou J, Kapsalaki E, Bizakis I, Fezoulidis I, Vassiou K. Vidian canal and sphenoid sinus: an MDCT and cadaveric study of useful landmarks in skull base surgery. Surg Radiol Anat 2020;42:589-601.
23. Kurt MH, Bozkurt P, Bilecenoğlu B, Kolsuz ME, Orhan K. Morphometric analysis of vidian canal and its relations with surrounding anatomic structures by using cone-beam computed tomography. Folia Morphol (Warsz) 2020;79:366-73.
24. Liu SC, Wang HW, Su WF. Endoscopic vidian neurectomy: the value of preoperative computed tomographic guidance. Arch Otolaryngol Head Neck Surg 2010;136:595-602.
25. Ozturan O, Yenigun A, Degirmenci N, Aksoy F, Veyseller B. Co-existence of the Onodi cell with the variation of perisphenoidal structures. Eur Arch Otorhinolaryngol 2013;270:2057-63.
26. Bahşi İ, Orhan M, Kervancıoğlu P, Yalçın ED. The anatomical and radiological evaluation of the Vidian canal on cone-beam computed tomography images. Eur Arch Otorhinolaryngol 2019;276:1373-83.
27. Mason EC, Hudgins PA, Pradilla G, Oyesiku NM, Solares CA. Radiographic Analysis of the Vidian Canal and Its

Utility in Petrous Internal Carotid Artery Localization. Oper Neurosurg (Hagerstown) 2018;15:577-83.
28. Connor SEJ, Thomas NWM, Shapey J. Localisation of the petrous internal carotid artery relative to the vidian canal on computed tomography: a case-control study evaluating the impact of petroclival chondrosarcoma. Acta Neurochir (Wien) 2022;164:1939-48.
29. Cascio F, Gazia F, D'Alcontres FS, Felippu AWD, Migliorato A, Rizzo G, Palmeri S, Felippu AWD, Lucanto MC, Costa S, Cascio F. The centripetal endoscopic sinus surgery in patients with cystic fibrosis: A preliminary study. Am J Otolaryngol 2023;44:103912.

Cite this article as: Gong W, Cao W, Zhang W, Xiang R, Xu Y. Imaging anatomy of the vidian canal and its clinical significance. Quant Imaging Med Surg 2023;13(12):8704-8728. doi: 10.21037/qims-23-1033

